Progress In Electromagnetics Research B, Vol. 50, 37–59, 2013

FINITE ELEMENT ANALYSIS AND EXPERIMENTAL STUDY OF THE NEAR-MAGNETIC FIELD FOR DETECTION OF ROTOR FAULTS IN INDUCTION MOTORS

Remus Pusca[1, 2, *], Raphael Romary[1, 2], Virgiliu Fireteanu[3, 4], and Andrian Ceban[1, 2]

[1]Laboratoire Systèmes Electrotechniques et Environnement (LSEE), France

[2]Université d'Artois, Technoparc Futura, Béthune 62400, France

[3]EPM_NM Laboratory, Romania

[4]Politehnica University, 313 Splaiul Independentei, Bucharest 060042, Romania

Abstract—This paper deals with the finite element analysis and experimental study concerning the influence of the broken bar and rotor dynamic eccentricity faults on the magnetic field outside a squirrel-cage induction motor. The spatial distribution of the magnetic field, the time variation of the magnetic flux density at a point outside the machine and the time variation of the electromotive force delivered by a coil sensor are evaluated based on the finite element models of the healthy and faulty states of the motor. The increase of amplitude from the healthy to the faulty states of some low frequency harmonics measured in the near-magnetic field is emphasized. For broken bar fault, the increase of the amplitudes of specific harmonics of the coil sensor electromotive force, with frequency lower than 25 Hz, is experimentally confirmed.

1. INTRODUCTION

Induction Motors (**IM**) are used in many industrial applications because they are characterised by high reliability, low cost per power unit, high power per volume unit and need very low maintenance. However, diagnosis methods able to detect the motor failures are necessary in order to increase the safety and the performances of

Received 12 February 2013, Accepted 25 March 2013, Scheduled 28 March 2013

* Corresponding author: Remus Pusca (puscaremus@hotmail.com).

electric drive systems [1]. Fault detection in induction motors has been widely investigated, using different techniques, such as those based on vibrations or current signature analysis [2–8]. A diagnosis technique which can detect a failure and prevent the total damage of the motor is therefore of great importance [9, 10]. Over the last decade different solutions have been investigated and the research in this field is still in permanent evolution [11–16]. Methods based on the analysis of external magnetic field have been recently developed. Their main advantages are the noninvasive investigation and the simplicity of implementation. The noninvasive evaluation of the motor healthy state is based on the property that any fault changes the magnetic field in the near vicinity of the machine [17–23]. In this context, this paper studies the influence of a broken bar fault and the rotor dynamic eccentricity in squirrel-cage induction motors. The analysis is carried out using the output voltage delivered by a simple magnetic flux coil sensor placed outside the motor. This analysis is focused on the low frequency harmonics of the magnetic field outside the motor, which are less attenuated than the fundamental or higher rank harmonics when they penetrate through the stator magnetic core and the motor frame.

Fault diagnosis methods are generally based on the comparison between a reference spectrum of a measured variable, corresponding to the healthy state of the motor, and the spectrum related to the faulty motor [24, 25]. The difficulty lies in the fact that the supposed healthy state is practically never known until the failure occurs, because appropriate measurements for the healthy machine characterization have not been recorded before.

This paper analyses the harmonics of the magnetic field outside the motor and the harmonics of the coil sensor output voltage obtained through the finite element model of the motor. This model computes the electromagnetic field inside and outside of the motor [26, 27] in healthy and faulty conditions. There are also presented complementary results issued from the experimental study of the near-magnetic field through the spectral analysis of the coil sensor output voltage. The interest of both finite element and experimental investigations from practical point of view is to detect two faults in squirrel-cage rotors: one broken bar and eccentricity. Moreover, compared to the analytical study, the use of finite element analysis also broadens the sphere of study using less simplifying assumptions. It allows one to separate or to combine different faults and to determine the tendency of harmonic variations at different operating conditions. However it must be specified that the initial state of any real motor is more or less different from the ideal healthy state. Consequently, the initial reference spectrum can be more or less different from the ideal reference

spectrum provided by the finite element model of the healthy motor.

The paper is organized as follows. The second section of the paper is focused on the presentation of the finite element model of a squirrel cage induction motor able to investigate the near-magnetic field for the ideal healthy motor and for different types of rotor faults. Next section analyzes the low frequency harmonic components of this magnetic field which are less attenuated by the metallic frame of the motor. The fourth section describes the experimental study of low frequency harmonics related to the influence of the broken rotor bar fault on the magnetic field outside the motor.

2. FINITE ELEMENT MODEL AND THE NONINVASIVE DETECTION OF ROTOR FAULTS

2.1. Description of the Motor Finite Element Model

The main electromagnetic phenomena characterising the steady state or transient operation of the usual squirrel cage induction motors are well enough reflected by a two-dimension finite element model. This is the case of healthy motors and faulty ones, with squirrel cage broken bars and/or a rotor eccentricity constant along the motor length.

The model is implemented in the Flux2D application. The geometry, the circuit model and the finite element mesh in Figs. 1(a)–(c), correspond to a $p = 2$ pole pairs motor of 4 kW, 400 V and $f = 50$ Hz supplied, which is used in the experimental study. The computation domain, infinitely extended, contains the stator and the rotor cores — magnetic and nonconductive regions (Fig. 1(a)), the stator slots — nonconductive, nonmagnetic coil regions with current density, the airgap of 0.5 mm thickness and many regions of solid conductor type — the rotor slots, the rotor shaft and the motor frame of 5 mm thickness. Moreover, a dynamic eccentricity of 40% of the airgap width can be imposed.

The nonlinear magnetic cores are characterised by the saturation at 2 T, the initial value of the relative magnetic permeability 4000 and the curvature coefficient 0.3. The squirrel-cage is aluminium made of resistivity 0.027 μΩm and the frame of the motor is Al-Si alloy made of resistivity 0.045 μΩm. The rotor shaft is made of magnetic steel with resistivity 0.2 μΩm, saturation 1.8 T and initial relative permeability 1800. The broken bar is simulated through the 0.027 Ωm value of the resistivity in the corresponding region.

The geometry shown in Fig. 1(a) includes also the two coil regions *Sensor Ox* and *Sensor Oy* of the sensors for the evaluation of the radial, respectively azimuth components of the magnetic field outside the motor. The magnetic vector potential $A(x, y, z, t)$ — the state

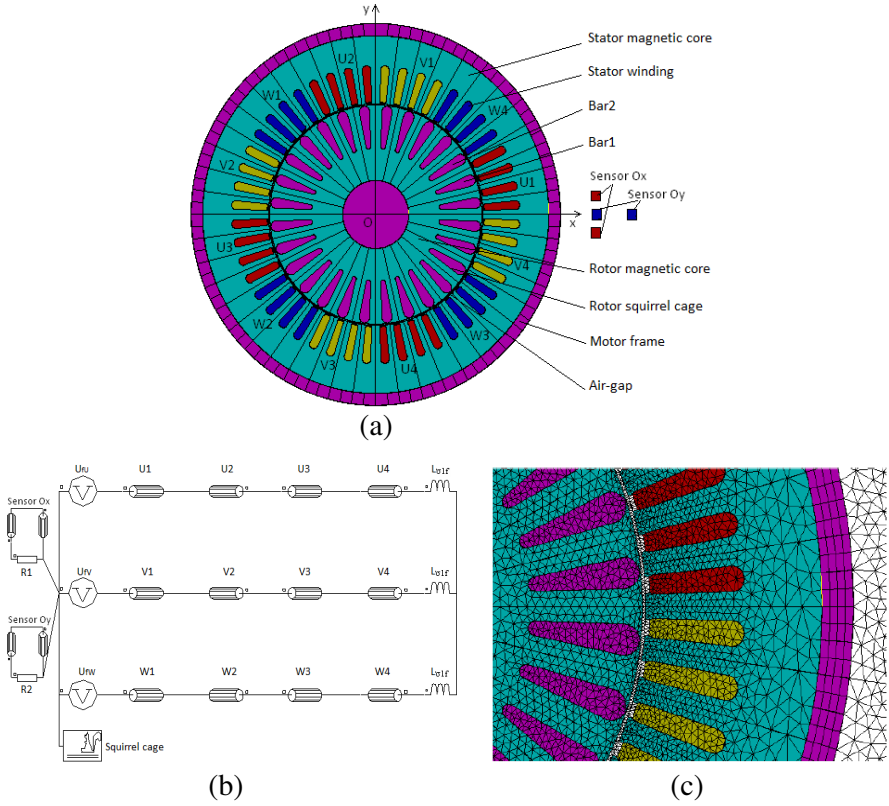

Figure 1. Finite element model: (a) geometry; (b) circuit model; (c) mesh zoom.

variable of the electromagnetic field, satisfies the equations [28–30]:

$$\begin{cases} \text{curl}[1/\mu \cdot \text{curl}A] + (\partial A/\partial t)/\rho = J_s(x, y, z, t) \\ \text{div}A = 0 \end{cases} \tag{1}$$

where μ is the magnetic permeability, ρ the resistivity, and J_s the current density in the stator slots. The term $(\partial A/\partial t)/\rho$ is the density of the induced current, which is different from zero only in the solid conductor regions. The vector quantity that is the source current density has the structure $J_s[0, 0, J_s(x, y, t)]$. As consequence, the vector potential $A_s[0, 0, A_s(x, y, t)]$ is oriented along the Oz axis, normally oriented with respect to Fig. 1(a), and not depends on the coordinate z. In this 2D context, the second equation of (1) is implicitly satisfied.

The attached circuit model, shown in Fig. 1(b), contains twelve

circuit components of stranded coil type, which correspond to the four zones of each of the three phases of the stator winding. The leakage inductances $L_{\sigma 1f}$ correspond to the part of the stator winding which is outside the stator magnetic core represented by the 2D model of the motor. The supply sources, U_U, U_V, U_W, are the phase-to-null voltages of the symmetric three phase motor supply. The macro-component *Squirrel cage* reflects the rotor bars and the electric parameters of the squirrel cage outside the rotor magnetic core. The circuit model of the motor includes also four circuit components of stranded coil type that correspond to the *Sensor Ox* and *Sensor Oy* regions in the geometry and the two resistors $R1$ and $R2$ for sensor output voltage evaluation.

Since the main interest of the finite element model is the non-invasive fault diagnosis based on magnetic field outside the motor, the mesh of the computation domain shown in Fig. 1(c), is fine enough inside and outside the motor. It is also fine enough in the regions of solid conductor type, in order to have a good accuracy of the numerical solution.

Two models associated with the rotor motion can be considered: motion model with constant speed 1425 rpm ($s = 0.05$), and the complementary motion model with constant mechanical load 26 Nm.

The step-by-step in time domain analysis of the electromagnetic field considers the time step value of 1 ms. The steady state motor operation is reached in about 600 ms. The time interval $(0.6 \ldots 1.4)$ s is considered for the result analysis. The time interval 0.8 s corresponds to the double of the period $1/(sf) = 0.4$ s of the electromagnetic field outside the motor when the machine rotates at 1425 rpm.

2.2. Lines of the Near-magnetic Field

The study of the faults influence on the near-magnetic field takes into account the operation at constant mechanical load. Four cases have been considered: healthy motor, one broken bar, rotor eccentricity and both faults.

It is observed that the motor speed has very small oscillations in case of the heathy motor, in the range $(1428.4 \ldots 1428.8)$ rpm. These oscillations, at $2sf$ frequency, increase for the faulty motor. In case of the broken bar fault the speed oscillates in the range $(1423.8 \ldots 1428.5)$ rpm, for rotor eccentricity fault in the range $(1428.3 \ldots 1428.9)$ rpm and for both faults in the range $(1424.0 \ldots 1429.2)$ rpm. The motor speed oscillations have been experimentally proved for the broken bar fault [12, 31, 32].

The maps of the magnetic field lines outside the motor for the time steps 0.6 s, 1.0 s and 1.4 s are presented in Fig. 2 for the healthy motor, in Fig. 3 for one broken bar, in Fig. 4 for rotor eccentricity and

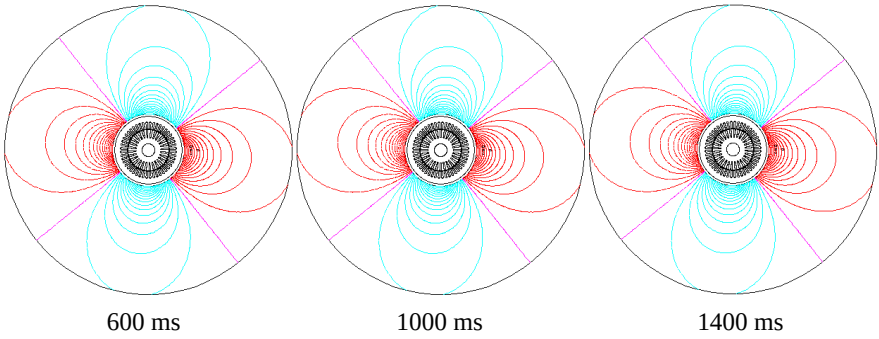

Figure 2. Lines of the near-magnetic field for the healthy motor.

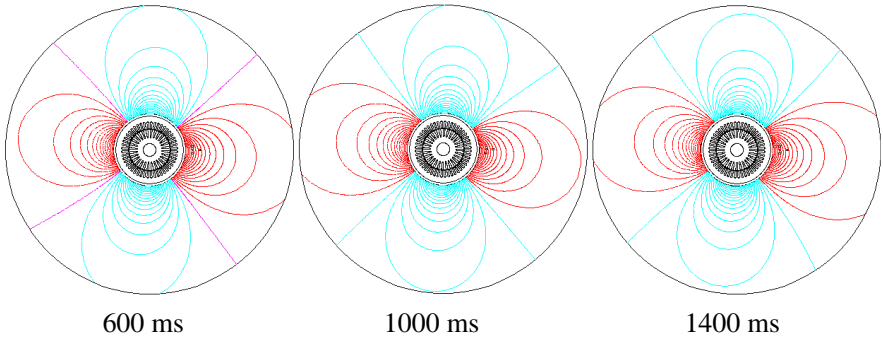

Figure 3. Lines of the near-magnetic field for the motor with one broken bar.

in Fig. 5 for both faults. As Figs. 2–5 show, the approximate period of the near-magnetic field is the double of the period of rotor currents (0.8 s). That explains the choice for 600 ms, 1000 ms and 1400 ms for the magnetic field lines representation.

In case of the healthy motor (Fig. 2), the lines of the magnetic field outside the motor are identical for the four poles. For one broken bar, there are slight differences from one pole to another (Fig. 3). If the number of broken bars and the number of motor poles increase, the dissymmetry becomes higher [33–39].

As Fig. 4 shows, the rotor eccentricity fault has an impact on the magnetic field distribution higher than the broken bar fault. If the two faults are present (Fig. 5), the changes in the magnetic field lines distribution are very significant.

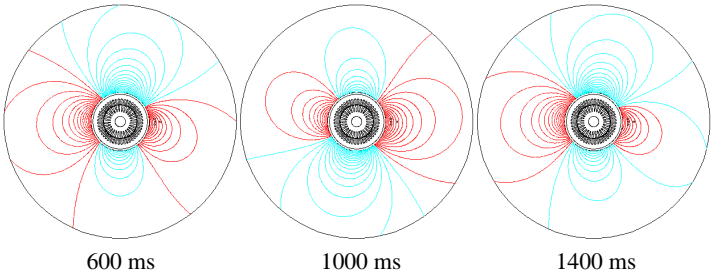

Figure 4. Lines of the near-magnetic field for the motor with rotor eccentricity.

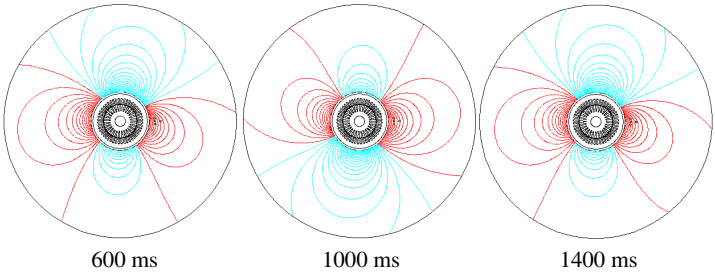

Figure 5. Lines of the near-magnetic field for one broken bar and rotor eccentricity.

2.3. Influence of the Rotor Faults on the Time Variation of the Magnetic Flux Density

The time variation of the both components of the magnetic flux density is analyzed: the radial component *Bx* at the center of the *Sensor Ox* and the azimuth one *By* at the center of the *Sensor Oy*. The time variations of these variables are presented in the Fig. 6 for the healthy motor, in Fig. 7 for the one broken bar fault, in Fig. 8 for the rotor eccentricity fault and in Fig. 9 for both faults. It can be observed that the amplitudes of *Bx(t)* and *By(t)* stay practically constant for the healthy motor.

For all faulty cases, the amplitude of the two components of the magnetic flux density changes more all less in time. Consequently, the Fast Fourier Transform (**FFT**) analysis in the frequency domain, oriented toward the low frequency range (less than 10 Hz), is further considered.

Assuming the low frequency harmonics of the magnetic field outside the motor are in connection with similar harmonics of the

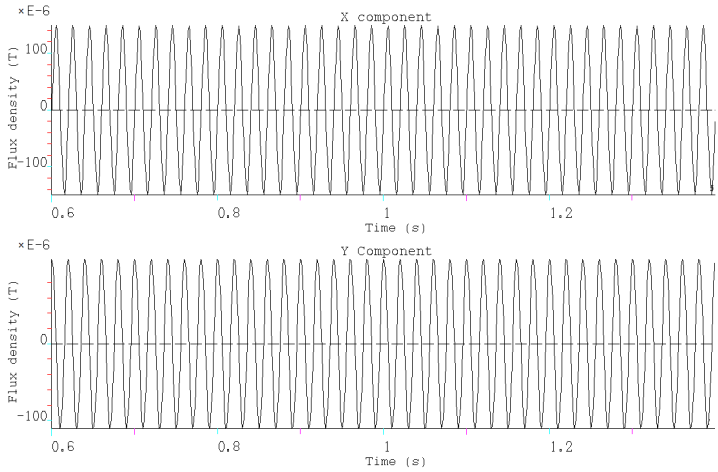

Figure 6. Time variation of the magnetic flux density for the healthy motor.

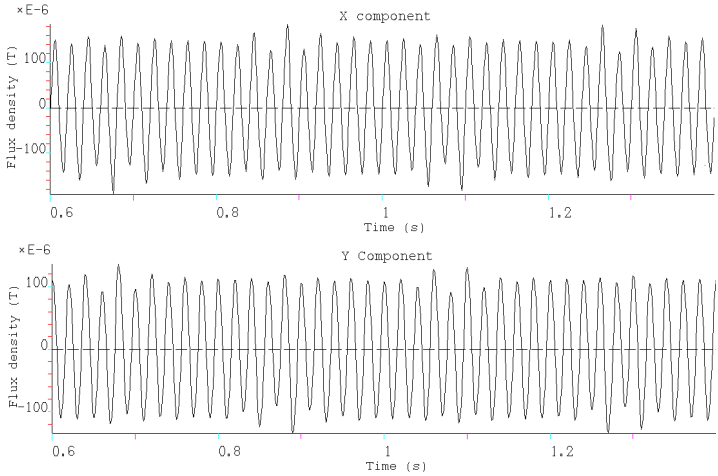

Figure 7. Time variation of the magnetic flux density for the one broken bar fault.

magnetic field inside the motor, the interest for the low frequency range comes from the fact that the corresponding harmonics are less affected by the attenuation effect of the motor metallic frame.

The comparison of eight low frequency harmonics for the healthy motor (0BC) and for the motor with one broken rotor bar (1BC) in the Fig. 10 shows the increase of the amplitude of these harmonics of the

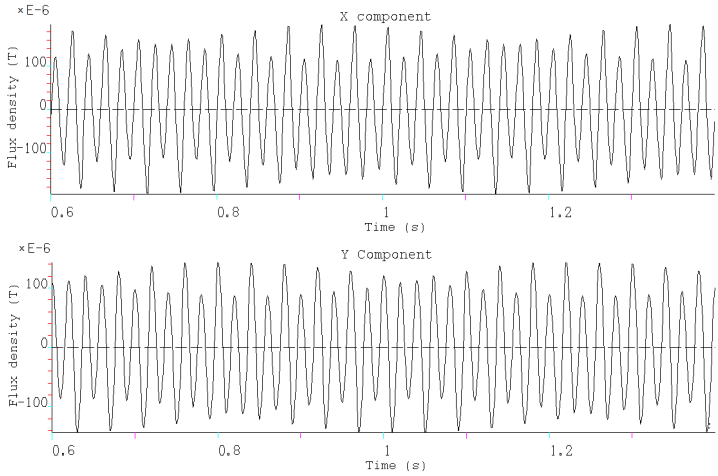

Figure 8. Time variation of the magnetic flux density for the rotor eccentricity fault.

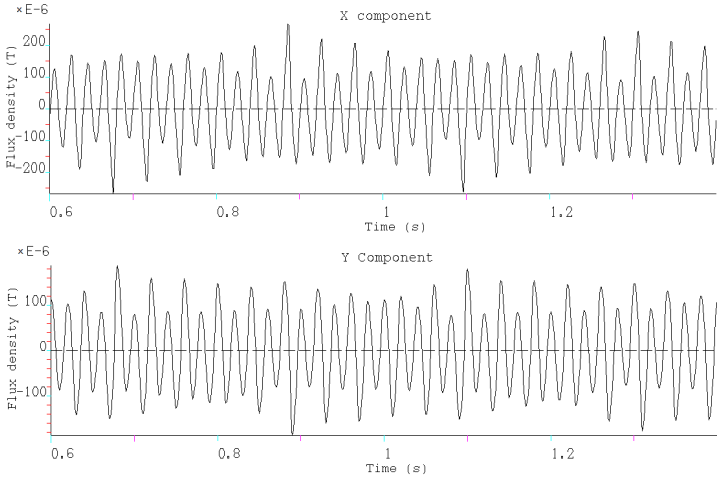

Figure 9. Time variation of the magnetic flux density for both faults — one broken bar and rotor eccentricity.

near magnetic field when the fault appears. The 1.25 Hz and 6.25 Hz are the most important harmonics for the broken bar detection of the motor under study. The harmonic of the azimuth component B_y of the magnetic field, with the frequency $sf = 2.5$ Hz [20] — marked in Fig. 10, is much more affected by the fault than the same harmonic of the radial component B_x.

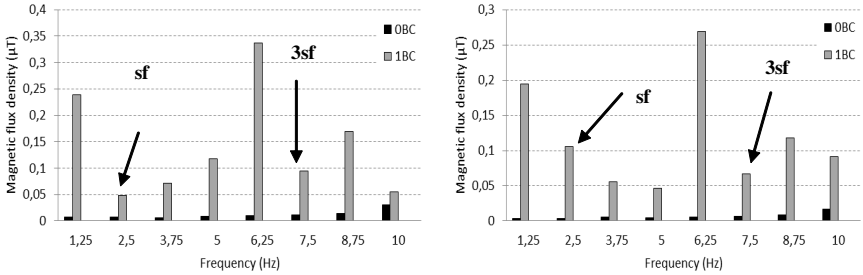

Figure 10. Amplitudes of low frequency harmonics for healthy and for the one broken bar fault: (a) B_x harmonics; (b) B_y harmonics.

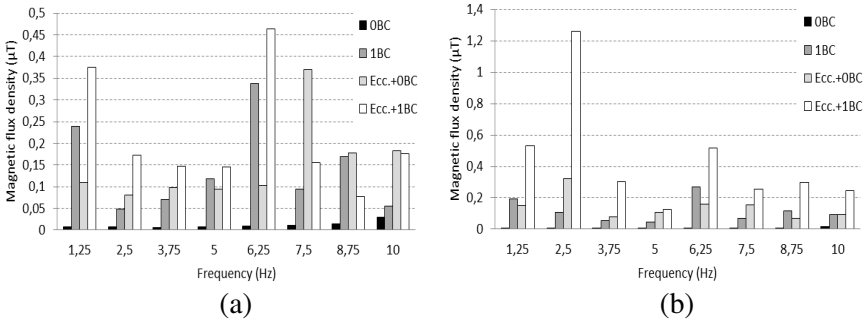

Figure 11. Amplitudes of low frequency harmonics for healthy and faulty motor: (a) B_x harmonics; (b) B_y harmonics.

As Fig. 11 shows, the increase of the amplitude of all eight low frequency harmonics of the two components of the magnetic flux density is also evident when the rotor eccentricity exists (Ecc + 0BC) or in case of both motor faults (Ecc + 1BC). Related to the B_x component in Fig. 11(a), the most important increase characterises the amplitude of the 6.25 Hz harmonic. In case of the eccentricity fault only, it appears that the 7.50 Hz harmonic is the highest.

It appears that the amplitude of the 2.5 Hz (sf) harmonic of the B_y component is higher than this of the B_x component, Fig. 11(b). Therefore, this low frequency harmonic should be considered for motor fault diagnosis.

Since the amplitudes of the low frequency harmonics related to the two flux density components of the near-magnetic field are in the order of some μT, the fault detection based on these quantities can

be easily influenced by external perturbations. This drawback can be overcome by using the output voltage delivered by the coil sensors.

3. THE ROTOR FAULT AND THE LOW FREQUENCY HARMONICS OF THE COIL SENSORS OUTPUT EMF

The time variation and the harmonics of the output electromotive force (emf) of the coil sensor *Sensor Ox*, are presented in Fig. 12 for the healthy motor at constant speed, in Fig. 13 for one broken rotor bar at constant speed and in Fig. 14 for one broken bar at constant load. The abscise axis of these figures contains the order number of harmonics of the output emf. The frequency of the harmonics in [Hz] is obtained by multiplying this number with 1.25.

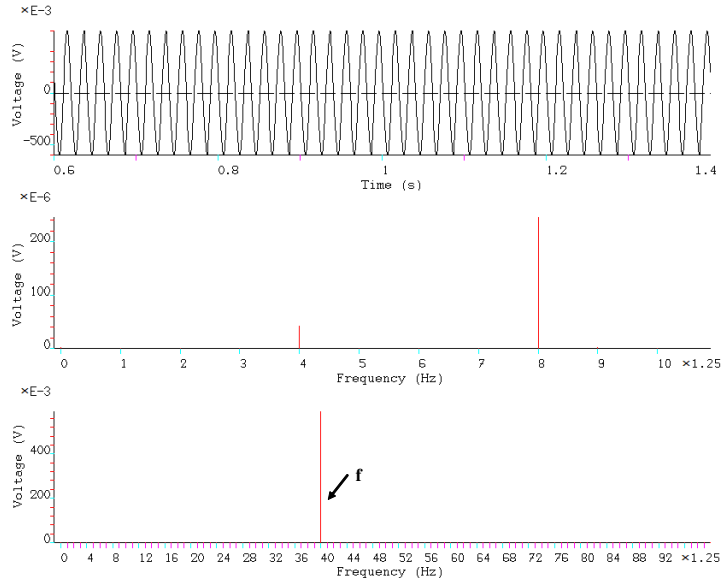

Figure 12. Time variation (up) and FFT spectrum (down) of *Sensor Ox* output emf for healthy motor and constant speed.

The corresponding rms values of the output emf are respectively 421.3 mV, 427.2 mV and 428.1 mV. Very small differences also characterise the harmonic number 40, with the frequency $f = 50$ Hz of the motor electric power supply.

Contrariwise, the spectra and the amplitudes of the low frequency harmonics, of 1.25 Hz, 2.5 Hz, 3.75 Hz, 12.5 Hz, observed in Figs. 12–14 (middle), are completely different for the faulty motor with one

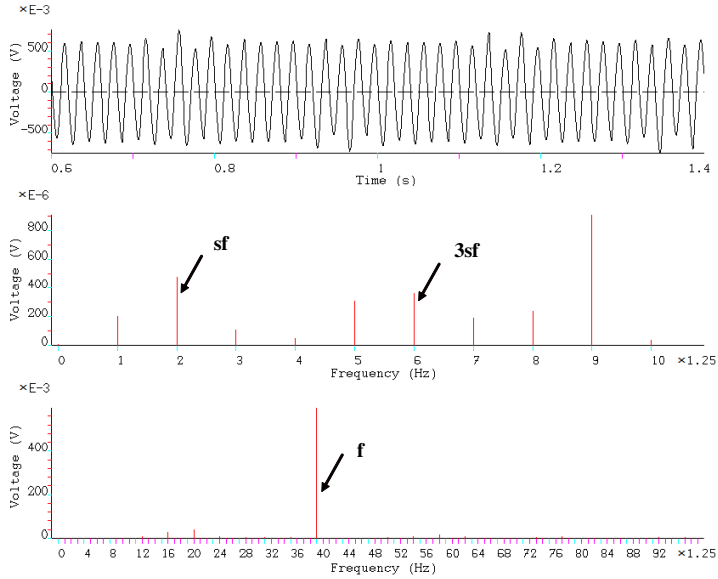

Figure 13. Time variation (up) and FFT spectrum (down) of *Sensor Ox* output emf for one broken bar and constant speed.

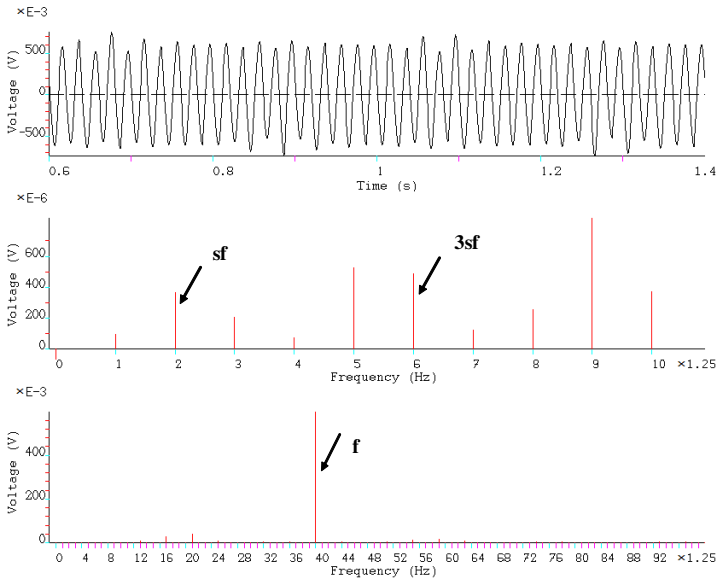

Figure 14. Time variation (up) and FFT spectrum (down) of *Sensor Ox* output emf for one broken bar and constant load.

broken bar than for the healthy motor. The harmonic number 2, with the frequency $sf = 2.5\,\text{Hz}$, which is practically nonexistent in case of the healthy motor (Fig. 12), has the amplitude around $500\,\mu\text{V}$ for one broken bar and constant speed, and around $400\,\mu\text{V}$ for one broken bar and constant load. For simulated cases we can observe the factional harmonics in the spectrum of the magnetic flux density (Figs. 10 and 11) and of the sensor emf (Figs. 13 and 14). These correspond to the solving step imposed at the half value (1.25 Hz) of the sf frequency (2.5 Hz), so that the FFT algorithm returns a result for all the spectral lines, separate of 1.25 Hz. More accurate results could be obtained with a higher frequency resolution but it would require a high computation time. We can also remark that comparing Figs. 10 and 11 to Figs. 13 and 14, it appears that the transfer function between flux density and electromotive force, decreases the factional harmonics.

The appearance of the low frequency components in the spectrum of the coil sensors output emf is due the combination of phenomena such as: broken bar, eccentricity, speed variation and magnetic saturation. The interaction of these phenomena is presented in [20] with an analytical approach. Based on the analysis of the axial flux, this study shows the great influence of the rotor speed oscilations. This variation occurs at $2sf$ frequency with the broken bar fault. Very low amplitudes of speed oscillations, less than 5 rpm, are able to generate low frequency harmonics with significant amplitude. The analysis of the axial field requires three-dimension finite element model. However, equivalent properties of the axial field can be refound in the two-dimension analysis because the axial field can be seen as an extension of the radial magnetic field. Therefore, similar frequencies exist in the both approaches.

4. EXPERIMENTAL STUDY OF ONE BROKEN BAR FAULT

It must be noticed that the results of the experimental study presented in this section can be compared only qualitatively with the similar results issued from the two-dimension finite element analysis of the near-magnetic field. The main reasons are as follows:

a) the two-dimension finite element model corresponds to an infinitely extension of the induction motor in the axial direction, where there is no axial component of the magnetic field. The radial, azimuth and axial components of the magnetic field in a real motor are not independent each other, they represent parts of the real three-dimension magnetic field;

b) the metallic frame of the motor in the finite element model has different geometry and material properties than in the motor used in the experimental study. The inner side of the two motors has the same geometry and physical properties;

c) the geometries of the coil sensor and the distance from the motor axis in the finite element model and in the experimental study are different.

4.1. Bench Test

The bench test in Fig. 15 was used for the experimental study of the rotor broken bar fault on the harmonics of the output emf of coil sensors.

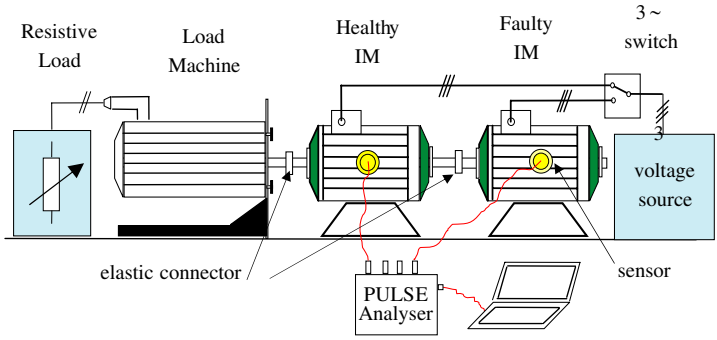

Figure 15. Experimental bench test.

This bench includes two 3-phase squirrel cage induction motors, 4 kW, 1500 rpm, rated supplied 380 V, 50 Hz, coupled to a permanent magnet synchronous generator. One motor is the healthy machine and the other is the faulty machine with one broken bar of the squirrel cage. The synchronous generator is connected to a variable resistive load.

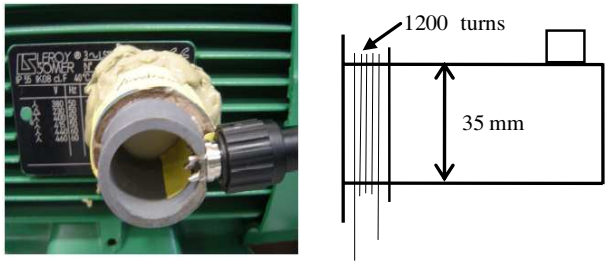

Figure 16. The coil sensor for the magnetic field investigation in the **IM** neighboring.

The circular coil sensor shown in Fig. 16, with 35 mm diameter and 1200 turns, was built for the investigation of the magnetic field outside the AC electrical machines.

The frequency response given in Fig. 17, shows a resonance frequency around 93 kHz for the coil sensor, much higher than the range of low frequencies investigated by the experimental study.

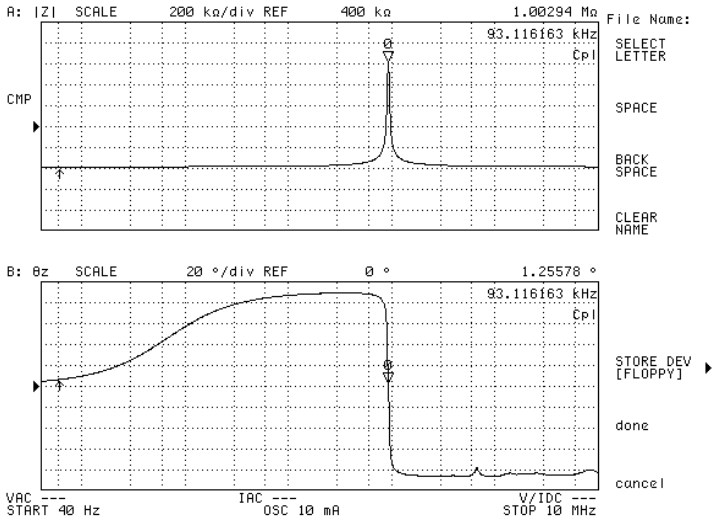

Figure 17. Frequency response of the coil sensor for experimental study.

4.2. Coil Sensor Positions, the Output emf Analysis

The magnetic field created by the electric currents in the stator and rotor electric circuits outside an induction machine with axial oriented stator and rotor slots can be qualified as:

- **radial field,** Fig. 18(a), whose lines are included in planes perpendicular to the machine axis. The lines of this field are composed of a normal and a tangential component related to the motor frame.
- **axial field,** Fig. 18(b), in planes that contains the machine axis. There are two points along the lines of this field where the magnetic field vectors are axially oriented, respectively are parallel with the motor axis.

The **radial field** is generated by the parts of the electric circuits having axial orientation, respectively by the sections of the electric

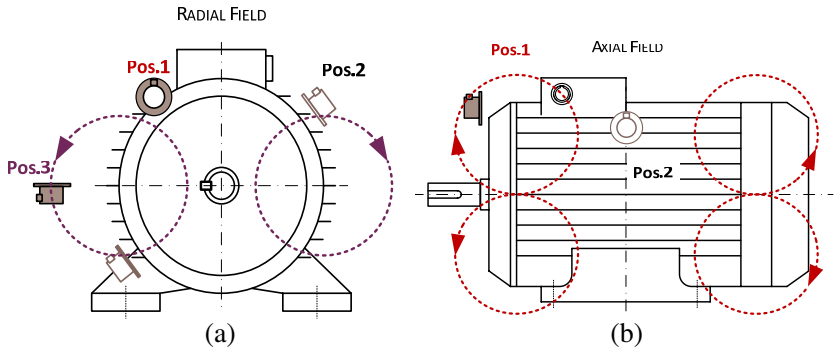

Figure 18. Magnetic field outside the motor: (a) radial field; (b) axial field.

circuits placed in the stator and rotor slots. The **axial field** is mainly associated with the electric currents in the frontal sections of the stator coils (winding head) and by the currents in the rotor end rings.

Figure 18 shows different positions of the coil sensor for the study of the near magnetic field. Accordingly to the position and orientation of the coil sensor with respect machine frame, the sensor is more or less sensitive to one or another component of the **radial field** and the **axial field**. Thus:

- in the *Pos.*1 coil sensor position, the axial component of the field produced by the winding head is investigated,
- in the *Pos.*2, the sensor measures the normal components of the **radial** and **axial fields**,
- in the *Pos.*3, the sensor measures the tangential component of the **radial field** only. In that position, the sensor is not sensitive to the **axial field**.

The *Sensor Ox* position in the Fig. 1, corresponds to the **Pos.2** position in the Fig. 18(a) and the *Sensor Oy* position corresponds to the **Pos.3** position.

The output emf of the coil sensor is connected to a Brüel & Kjær PULSE analyzer, which performs the FFT signal processing and provides its spectrum with specific low frequency harmonics. The results of signal processing are therefore sent to a computer for viewing and recording.

4.3. Results of the Experimental Study

The output emf of the coil sensor placed in the **Pos.2** position is presented in Fig. 19 for the healthy motor and in Fig. 20 for the faulty

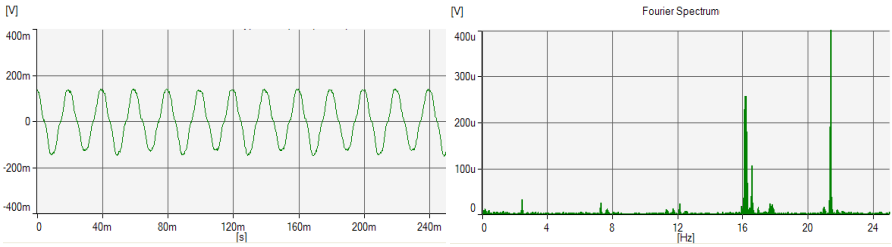

Figure 19. Time variation of the coil sensor emf and the FFT spectrum in case of the healthy motor, with sensor placed in *Pos.*2.

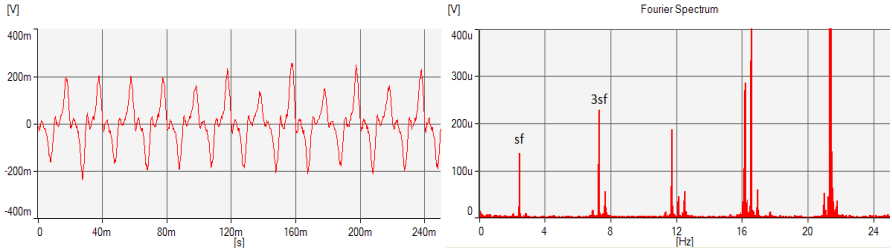

Figure 20. Time variation of the coil sensor emf and the FFT spectrum in case of the faulty motor, with sensor placed in *Pos.*2.

motor. The rotor speed is 1425 rpm, respectively the slip value is $s = 0.05$.

As Fig. 19 shows there are some low frequency harmonics of small amplitudes even in case of the healthy motor. The harmonic of sf and $3sf$ frequency are generated by the geometrical or/and physical imperfections of the tested healthy motor, maybe a small eccentricity, which are not considered in the finite element analysis.

In case of the faulty machine, with one broken bar (Fig. 20), the amplitude of the harmonics with the frequency $sf = 2.5$ Hz and $3sf = 7.5$ Hz clearly appear. Consequently, the detection of rotor bar faults based on the evaluation of the amplitudes corresponding to the harmonics sf and/or $3sf$ of the coil sensor output emf is experimentally confirmed.

Results given in Figs. 21 and 22 correspond to the ***Pos.3*** position of the coil sensor respectively for the healthy motor and for the faulty motor with one broken bar. The appearance of the sf and $3sf$ harmonics in the coil sensor output emf in faulty condition can be also observed. The comparison of the ***Pos.2*** and ***Pos.3*** results in the Figs. 19–22 proves a better visibility of the fault detection

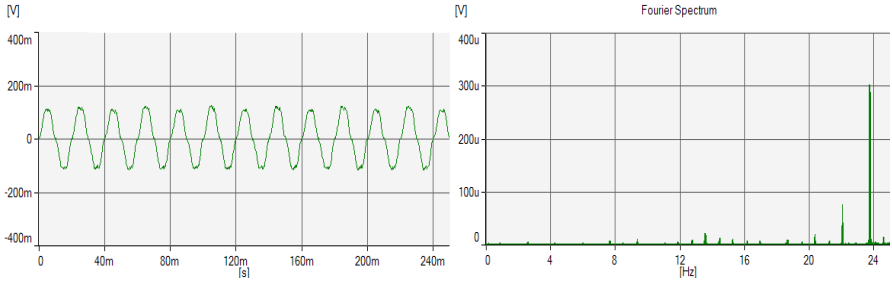

Figure 21. Time variation of the coil sensor emf and the FFT spectrum in case of the healthy motor, with sensor placed in *Pos.*3.

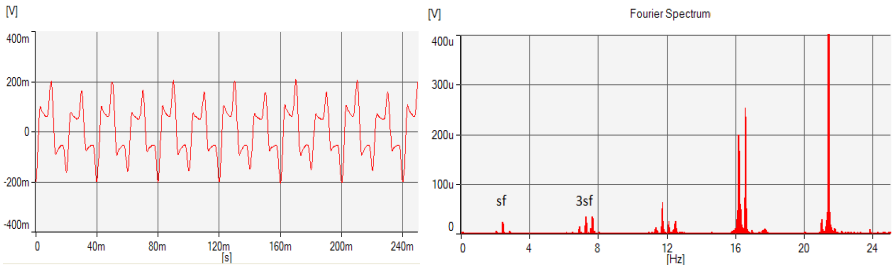

Figure 22. Time variation of the coil sensor emf and the FFT spectrum in case of the faulty motor, with sensor placed in *Pos.*3.

with the normal component of the magnetic field related to motor frame (***Pos.*2**) than with the tangential component (***Pos.*3**). Actually, ***Pos.*2** also measures a part of the axial field.

Comparing the measured results and the finite element ones, it may be remarked differences in amplitude. In addition to the remarks given in the introduction of Section 4, these differences are also due to perfect simulation model, which does not take into account the manufacturing asymmetries, as they are not known. The factional harmonics presented in simulated spectrum correspond to the solving step imposed and more accurate results could be obtained with a higher frequency resolution.

Although these imperfections and asymmetries exist, a qualitative study between the both methods is possible. So the finite element analysis gives the tendency of the harmonics sf and $3sf$ evolution for different operating conditions (load variation, sensor position) and gives the possibility to perform a comparative study between the spectra of the sensor output emf obtained by simulation and by measurement. It also enables to analyze the individual or combined

influence of different faults in the changes of the emf spectrum and to identify new specific harmonics related to other faults.

5. CONCLUSION

The finite element analysis and the associated numerical models represent not only a modern technology of induction motor computer aided design and optimisation but also a powerful and very efficient orientation in the study and detection of different faults associated with the motor operation. In this context, the paper emphasizes the changes in the spatial distribution of the time dependent magnetic field in the neighbouring of a squirrel cage motor due to the broken bar and rotor eccentricity faults. These faults induce the appearance of specific harmonics in the spectrum of the output voltage delivered by a coil sensor, with frequency much lower than the rated frequency of motor power supply. It is only the finite element analysis, able to consider the ideal healthy machine in the study of individual or cumulative effects of different faults. This can be the reference state of the motor for the experimental faults investigation, respectively for the online detection of motor faults.

For an induction motor in operation, the study of the healthy and faulty states based on the finite element model establishes the configuration and position of sensors, the most appropriate harmonic of the output emf and much other useful information in the optimal design of online fault detection. The increase of the amplitude of sensitive harmonics of the coil sensor output emf in case of the broken bar fault in the studied induction motor was experimentally confirmed.

6. NOMENCLATURE

p	Number of pole pair,
f	Supply frequency, Hz,
μ	Magnetic permeability, H/m,
$L_{\sigma 1f}$	Inductance corresponding to the part of the stator winding outside the stator magnetic core, H,
ρ	Resistivity, Ωm,
J_s	Current density in the stator slots, A/m^2,
t	Time, s,
s	Slip, between 0 and 1,
B_x	Radial component of the magnetic flux density, Wb,

B_y	Azimuth component of the magnetic flux density, Wb,
emf	Electromotive force, V,
FFT	Fast Fourier Transform,
0BC	No broken rotor bar,
1BC	Motor with one broken rotor bar,
Ecc	Motor with rotor eccentricity,

REFERENCES

1. Seungdeog, C., B. Akin, M. M. Rahimian, and H. A. Toliyat, "Performance-oriented electric motors diagnostics in modern energy conversion systems," *IEEE Trans. on Ind. Electron.*, Vol. 59, No. 2, 1266–1277, Feb. 2012.
2. Lecointe, J. P., B. Cassoret, and J. F. Brudny, "Distinction of toothing and saturation effects on magnetic noise of induction motors," *Progress In Electromagnetics Research*, Vol. 112, 125–137, 2011.
3. Cassoret, B., J. P. Lecointe, and J. F. Brudny, "Influence of the pole number on the magnetic noise of electrical AC machines," *Progress In Electromagnetics Research B*, Vol. 33, 83–97, 2011.
4. Benbouzid, M. E. H., "A review of induction motors signature analysis as a medium for faults detection," *IEEE Trans. on Ind. Electron.*, Vol. 47, No. 5, 984–993, Oct. 2000.
5. Henao, H., H. Razik, and G. A. Capolino, "Analytical approach of the stator current frequency harmonics computation for detection of induction machine rotor faults," *IEEE Trans. on Ind. Appl.*, Vol. 41, No. 3, 801–807, May/Jun. 2005.
6. Lim, W. Q., D. H. Zhang, J. H. Zhou, P. H. Belgi, and H. L. Chan, "Vibration-based fault diagnostic platform for rotary machines," *36th Annual Conference on IEEE Industrial Electronics Society (IECON 2010)*, 1404–1409, 2010.
7. Filippetti, F., G. Franceschini, C. Tassoni, and P. Vas, "AI techniques in induction machines diagnosis including the speed ripple effect," *IEEE Trans. on Ind. Appl.*, Vol. 34, No. 1, 98–108, Jan./Feb. 1998.
8. Khezzar, A., M. Y. Kaikaa, M. El Kamel Oumaamar, M. Boucherma, and H. Razik, "On the use of slot harmonics as a potential indicator of rotor bar breakage in the induction machine," *IEEE Trans. on Ind. Electron.*, Vol. 56, No. 11, 4592–4605, Nov. 2009.

9. Pouliezos, D. and G. S. Stavrakakis, *Real Time Fault Monitoring of Industrial Processes*, Kluwer, Norwell, MA, 1994.
10. Tavner, P., L. Ran, J. Penman, and H. Sedding, *Condition Monitoring of Rotating Electrical Machines*, 2nd Edition, IET, Stevenage, UK, 2008.
11. Bossio, G. R., C. H. De Angelo, J. M. Bossio, C. M. Pezzani, and G. O. Garcia, "Separating broken rotor bars and load oscillations on IM fault diagnosis through the instantaneous active and reactive currents," *IEEE Trans. on Ind. Electron.*, Vol. 56, No. 11, 4571–4580, Nov. 2009.
12. Nemec, M., K. Drobnic, D. Nedeljkovic, R. Fiser, and V. Ambrozic, "Detection of broken bar in induction motor using voltage pattern analysis," *IEEE Trans. on Ind. Electron.*, Vol. 57, No. 8, 2879–2888, Aug. 2010.
13. Sanchez, M. P., M. R. Guasp, J. A. A. Daviu, J. R. Folch, J. P. Cruz, and R. P. Panadero, "Instantaneous frequency of the left sideband harmonic during the start-up transient: A new method for diagnosis of broken bar," *IEEE Trans. on Ind. Electron.*, Vol. 56, No. 11, 4557–4570, Nov. 2009.
14. Bouzida, A., O. Touhami, R. Ibtiouen, A. Belouchrani, M. Fadel, and A. Rezzoug, "Fault diagnosis in industrial induction machines through discrete wavelet transform," *IEEE Trans. on Ind. Electron.*, Vol. 59, No. 9, 4385–4395, Sep. 2011.
15. Drif, M. and A. J. M. Cardoso, "Discriminating the simultaneous occurrence of three-phase induction motor faults and mechanical load oscillations by the instantaneous active and reactive power media signature analyses," *IEEE Trans. on Ind. Electron.*, Vol. 59, No. 3, 1630–1639, Mar. 2012.
16. Sanchez, M. P., M. R. Guasp, J. R. Folch, J. A. A. Daviu, J. P. Cruz, and R. P. Panadero, "Diagnosis of induction motor faults in time varying conditions using the polynomial phase transform of the current," *IEEE Trans. on Ind. Electron.*, Vol. 59, No. 4, 1428–1439, Apr. 2011.
17. Henao, H., C. Demian, and G. A. Capolino, "A frequency-domain detection of stator winding faults in induction machines using an external flux sensor," *IEEE Trans. on Ind. Appl.*, Vol. 39, 1272–1279, Sep./Oct. 2003.
18. Romary, R., R. Corton, D. Thailly, and J. F. Brudny, "Induction machine fault diagnosis using an external radial flux sensor," *The European Physical Journal — Applied Physics*, Vol. 32, 125–132, 2005.
19. Penman, J., H. G. Sedding, and W. T. Fink, "Detection and

location of interturn short circuits in the stator windings of operating motors," *IEEE Trans. on Energy Conversion*, Vol. 9, No. 4, 652–658, Dec. 1994.

20. Ceban, A., R. Pusca, and R. Romary, "Study of rotor faults in induction motors using external magnetic field analysis," *IEEE Trans. on Ind. Electron.*, Vol. 59, 2082–2093, May 2012.
21. Frosini, L., A. Borin, L. Girometta, and G. Venchi, "A novel approach to detect short circuits in low voltage induction motor by stray flux measurement," *20th International Conference on Electrical Machines (ICEM'12)*, 1536–1542, Sep. 2012.
22. Assaf, T., H. Henao, and G.-A. Capolino, "Simplified axial flux spectrum method to detect incipient stator inter-turn short-circuits in induction machine," *2004 IEEE International Symposium on Industrial Electronics*, Vol. 2, 815–819, Ajaccio, France, 2004.
23. Cabanas, M. F., M. G. Melero, G. A. Orcajo, F. Rodriguez Faya, and J. Solares Sariego, "Experimental application of axial leakage flux to the detection of rotor asymmetries, mechanical anomalies and interturn shortcircuits in working induction motors," *Proc. of International Conference on Electrical Machines, ICEM'98*, 420–425, Istanbul, Turkey, Sep. 2–4, 1998.
24. Fišer, R. and S. Ferkolj, "Magnetic field analysis of induction motor with rotor faults," *COMPEL*, Vol. 17, No. 1–3, 206–211, 1998.
25. Bellini, A., A. Yazidi, F. Filippetti, C. Rossi, and G.-A. Capolino, "High frequency resolution techniques for rotor fault detection of induction machines," *IEEE Trans. on Ind. Electron.*, Vol. 55, No. 12, 4200–4209, Dec. 2008.
26. Reece, A. B. J. and T. W. Preston, *Finite Element Methods in Electrical Power Engineering*, Oxford University Press, 2000.
27. Kappatou, J., C. Marchand, and A. Razek, "Finite element analysis for the diagnosis of broken bars in 3-phase induction machines," *Studies in Applied Electromagnetics and Mechanics*, Vol. 27, 348–353, 2006.
28. Ceban, A., "Global diagnostic method of electrical machines," Doctoral Thesis, LSEE, Université d'Artois, Bethune, France, 2012.
29. Fireteanu, V., T. Tudorache, and P. Taras, "Finite element diagnosis of squirrel cage induction motors with rotor bar faults," *Proc. OPTIM Conf.*, 1–6, Brasov, Romania, 2006.
30. Fireteanu, V. and P. Taras, "Teaching induction machine

through finite element models," *18th International Conference on Electrical Machines, ICEM*, 1–6, Vilamoura, Portugal, Sep. 6–9, 2008.

31. Yazidi, A., H. Henao, G. A. Capolino, M. Artioli, F. Filippetti, and D. Casadei, "Flux signature analysis: An alternative method for the fault diagnosis of induction machines," *2005 IEEE Russia Power Tech*, 1–6, St. Petersburg, Russia, 2005.
32. Trzynadlowski, A. M., M. Ghassemzadeh, and S. F. Legowski, "Diagnosis of mechanical abnormalities in induction motors using instantaneous electric power," *IEEE Trans. on Energy Conversion*, Vol. 14, 1417–1423, Dec. 1999.
33. Kuptsov, V. V., A. S. Sarvarov, and M. Y. Petushkov, "A new approach to analysis of induction motors with rotor faults during startup based on the finite element method," *Progress In Electromagnetics Research B*, Vol. 45, 269–290, 2012.
34. Kia, S. H., H. Henao, G.-A. Capolino, and C. Martis, "Induction machine broken bars faults detection using stray flux after supply disconection," *32nd Annual Conference on IEEE Industrial Electronics, IECON*, 1498–1503, Paris, France, 2006.
35. Negrea, M. D., "Electromagnetic flux monitoring for detecting faults in electrical machines," Doctoral Dissertation at Helsinki University of Technology, Laboratory of Electromechanics, Nov. 2006.
36. Fireteanu, V., P. Taras, R. Romary, R. Pusca, and A. Ceban, "Effects of rotor faults on operation parameter and the low frequency harmonics of the magnetic field outside induction motors," *XVth International Symposium on Electromagnetic Fields, ISEF*, Paper PS4.9, Funchal, Madeira, Portugal, Sep. 1–3, 2011.
37. Faiz, J., B. M. Ebrahimi, and M. B. B. Sharifian, "Time stepping finite element analysis of broken bars fault in a three-phase squirrel-cage induction motor," *Progress In Electromagnetics Research*, Vol. 68, 53–70, 2007.
38. Fireteanu, V. and P. Taras, "Diagnosis of induction motor rotor faults based on finite element evaluation of voltage harmonics of coil sensors," *Proc. of IEEE Sensors Applications Symposium*, 1–5, Brescia, Italy, Feb. 7–9, 2012.
39. Fireteanu, V. and P. Taras, "Influence of the magnetic steel encasing of induction motors on the efficiency of the rotor faults diagnosis based on the harmonics of the coil sensors output voltage," *2012 XXth International Conference on Electrical Machines (ICEM)*, 1745–1750, Marseille, France, Sep. 2–5, 2012.